Article citation info:
Aoyagi T, Wakasugi T, Tsuru D, Tashima H. Analysis of effects of pre-chamber orifices on torch flame behaviours in lean-burn gas engines. Combustion Engines. 2024;199(4), 3-14. https://doi.org/10.19206/CE-188112

Takahide AOYAGI
Takuya WAKASUGI
Daisuke TSURU
Hiroshi TASHIMA

Combustion Engines
Polish Scientific Society of Combustion Engines

Analysis of effects of pre-chamber orifices on torch flame behaviours in lean-burn gas engines

ARTICLE INFO

Received: 5 March 2024
Revised: 31 March 2024
Accepted: 29 April 2024
Available online: 9 July 2024

Fuel conversion from heavy oil to natural gas is favoured as a quick remedy for GHG reduction from industrial engines in ship propulsion and power generation fields thanks to fewer carbon contents in natural gas. In medium-speed gas engines, the ejection of torch flame from a pre-chamber is often used to promote flame propagation within a main combustion chamber. Although orifice specifications affect the ejection behaviour of the torch flame and the following combustion in the main chamber, the effects are difficult to fully understand. Some of the authors developed a constant-volume combustion vessel that simulated the combustion chamber around the top dead centre of a pre-chamber type gas engine and observed the effects of orifice specifications on the torch flame ejection and the combustion in the main chamber. Still, the correlation was not concluded due to the lack of physical examination. In the paper, the above measurement results were confirmed by using RANS-type CFD considering the larger scale of the target engines, and the physical background of the effects of orifice specifications was successfully reproduced.

Key words: *gas engine, pre-chamber, torch flame, CFD simulation, combustion visualization*

1. Introduction

Many countries that are signatories to the Paris Agreement have set their action plans to achieve carbon neutrality (CN) by 2050, and progress is being made in the development of electrification [6] and e-fuels [11] to decarbonize prime movers in the field of land transportation. More generous GHG reduction targets have been set for off-road power sources, such as industrial engines and marine engines, because of their long continuous operating time, and high average engine load, which results in the difficulty in electrification. However, IMO/MEPC80 in 2023 [12] declared GHG reductions in the marine sector should be in line with other sectors. Since internal combustion engines will account for the majority even when CN is achieved, it is essential to shift to non-carbon-containing fuels such as ammonia and hydrogen by 2050. Due to the difference in combustion characteristics, long-term development is still necessary for practical application, and toward the short-term goal of halving GHG emissions by 2030, gas engines purely running on natural gas (NG) should be introduced on a large scale. After the widespread use of hydrogen fuel, continuous usage of gas engines with e-gas obtained from methanation could be the next option [1].

The mainstream of current marine gas engines burns a lean premixture of NG/air preferring the potential for reducing NO_x emissions without additional after-treatments and improving thermal efficiency thanks to the high degree of constant volume [10]. However, due to the lower combustion speed of the lean premixture, it is not easy to complete combustion in a combustion chamber of a larger scale, therefore a smaller ignition source or lower ignition energy may increase slippage of unburned methane and cycle-to-cycle variations [8]. For this reason, various enhanced ignition measures have been used for lean-burn gas engines instead of a usual open chamber with a spark plug. In medium-speed engines, so-called “precombustion chamber (PC) ignition” has been widely studied [14, 15, 20]. In the PC ignition, torch flames ejected through orifices bored at the tip of a PC are expected to promote the combustion in a main combustion chamber (MC) of the lean-burn gas engines, to shorten the distance for the premixed flame to propagate toward an end-gas zone, and to expand the stable combustion range free from misfire and knocking [5].

PC ignition systems are divided into passive PC ignition mainly used in lean-burn gas engines of ca. 200 mm or less in the bore, and active PC ignition so in lean-burn gas engines of more than 200 mm in the bore. The former is essentially a small dome-shaped cap attached over an electrode gap of a spark plug. There is no active scavenge of the inner PC gas, and the combustible MC mixture is the only fuel source that comes in through orifices drilled in the cap during a compression stroke. The latter has a PC of larger volume and an independent fuel supply path that realises the local stratification of the mixture concentration from PC to MC and strengthens the ignition potential and penetration of the torch flame. The active PC ignition is sometimes applied to small high-speed SI (Spark Ignition) engines and is named TJI (Turbulent Jet Ignition). It has been eagerly studied to promote combustion in small high-speed SI engines [3, 16, 25] and some extreme-performance engines [19].

Marine lean-burn gas engines, however, have significant geometric differences, such as a cylinder bore that exceeds the knock limit (ca. 100 mm in bore) of small SI engines, a smaller volume ratio of PC to MC and a multi-orifice layout in the PC tip. In addition, marine lean-burn gas engines are highly supercharged to keep the mean effective pressure compatible with their diesel substitutes under lean mixture conditions. These factors push the marine lean-

burn gas engines to have an independent fuel supply device in their PC. Even so, their stable operation range is strictly limited between a knocking limit on the richer mixture side and a misfiring limit on the leaner mixture side [21], and the active PC ignition for marine lean-burn gas engines [7, 13, 18] has been investigated and studied separately from the TJI for high-speed SI engines.

In general, because of high cost for experiments and measurements in large-scale engines, CFD simulation is intentionally utilized to support the development and design process of large lean-burn gas engines [2, 9, 24]. For example, in-cylinder phenomena such as the mixture formation in a PC [17] and pre-ignition initiated by lubricant oil droplets were numerically reproduced [23], although the validity of those simulations cannot be secured because of the lack of measurements including actual visualization of the torch flame in the whole of a MC. There are very few cases in which the validity of numerical predictions was examined by tracing back the effects of PC orifice specifications on the torch flame behaviours in the MC. Moreover, the validity of the simulation should be examined by comparing it with actual visualization data in consideration of the unsteady nature of lean-burn gas engine's in-cylinder phenomena such as mixture formation and two-stage ignition and combustion process.

Wakasugi et al. [22] developed a CVCV (Constant Volume Combustion Vessel) that simulated the combustion chamber around the top dead centre of a PC-type gas engine and observed the effects of orifice specifications on the torch flame ejection and the combustion process in the main chamber. Still, the correlation between them was not concluded due to the lack of physical examination.

In the study, the above measurement results were numerically confirmed by RANS-type CFD considering the larger scale of the target engines, and the mechanism of the effects of the orifice specification was successfully reproduced and extensively examined in non-combustible ambient conditions of the MC.

2. Experimental apparatuses and procedures

As mentioned, the measurement results acquired by Wakasugi et al. [22] were fully adopted for comparison with the CFD simulation, since they can be said to be rare attempts to investigate the effects of orifice specifications by visualizing ejection behaviour of the torch flame from a pre-chamber and the following combustion process in a main chamber. Although the duplication with the source literature is inevitable, the main points for measurement are described below.

Figure 1 and Table 1 show the cross-sectional views of the CVCV and its main specifications, respectively. The CVCV has a simple pancake-shaped internal volume as a Main combustion Chamber (MC) of ϕ240 mm in bore and 30 mm in height. The MC is nearly equivalent to the clearance volume of a typical medium-speed natural gas engine. A Pre-Chamber (PC) with orifices near its bottom is mounted on the centre of the CVCV top lid, and the configuration of the PC, such as orifice diameter and the number of orifices, can be changed by exchanging a PC tip attached to the bottom of the PC. The details of tested PC tips will be explained later. The PC and MC have independent air/fuel mixture intake paths, and each can supply air/fuel mixture of different compositions. The bottom wall of the MC is entirely made of quartz glass, and the inner surface of the MC top lid is mirror-polished. The layout realizes full optical access to in-chamber combustion phenomena from the bottom window and double-path type shadowgraph optics.

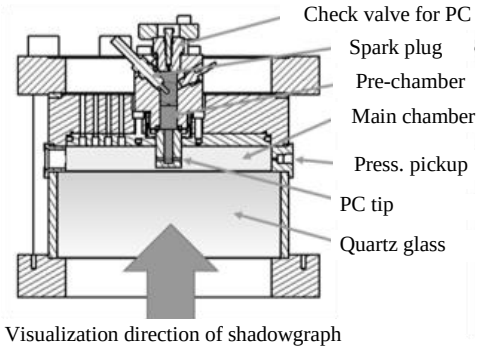

Fig. 1. Cross-sectional views of the CVCV

Table 1. Main specifications of CVCV

Main chamber ($D_{MC} \times H_{MC}$)	∅240 mm × 30 mm
Pre-chamber ($D_{PC} \times H_{PC}$)	∅20 mm × 65 mm (upper part w/o PC tip)
Optical window ($D_w \times t$)	∅260 mm × 100 mm Fused quartz glass
Max. in-chamber press.	10 MPa
Ignition device in PC	Spark plug
Mixture supply system	PC and MC separated

3. CFD setup and procedures

The 3D-CFD simulation by CONVERGE was tried to reproduce the above experimental results in the CVCV simulating combustion phenomena in a PC-type gas engine. Considering the larger scale of target medium-speed engines and the practical CFD usage in the design phase of future gas engines, a RANS turbulence scheme was adopted to save computational load and time. The details of the calculation setup and procedures are as follows.

The SAGE detailed chemical kinetics solver by Senecal [13] was adopted as the combustion model, and the spark ignition was modelled by the energy source model. The RNG k-ε model was adopted as a typical turbulence model in RANS simulation. In general, the SAGE combustion model calculates the elementary reaction rate while CFD solves the transport equation. However, to reduce the computational expense, this detailed chemistry was only activated in cells that passed the minimum temperature, and HC mole fraction specified in CONVERGE. In addition, the multi-zone chemistry model by Babajimopoulos [24] was used to expedite the detailed chemistry calculations. The reduced primary reference fuel mechanism was used to make efficient calculations. The standerd reaction mechanism in CONVERGE was used, and it consists of the reduced version of GRI-Mech1.2 by Andrei [9] with an enhanced Zeldvich mechanism embedded and consists of 26 species and 107 reactions for methane.

Figure 2 shows the initial meshing of the computational domain that models the internal volume of the CVCV. The PC and the MC of the CVCV are reproduced with cubic cells according to a rectangular Cartesian coordinate. In the case of the figure, the reference PC tip is set on the PC bottom. As shown in the figure, the orifices of the tested PC tips are horizontally bored.

The cell size was uniformly minimized at 1.0 mm in the internal space of the PC including the orifices. Considering the unburned gas and the torch flame ejection from the PC orifices, groups of cells of a truncated-cone shape were attached to the exit of orifices with a minimum diameter of about 8 mm and with a spread angle of about 30 degrees as shown in the figure. The initial number of cells was set to about 275,000. After the start of combustion in the MC, however, the Adaptive Mesh Refinement (AMR) was activated based on the local gradient in temperature and velocity between the cells, and the AMR automatically contracted the minimum cell size to 0.5 mm and increased the number of cells to a maximum of 150 million. All the wall temperatures surrounding the CVCV combustion chambers were set to 300 K. The heat loss to the wall surfaces was predicted by the turbulent heat transfer model based on the boundary layer treatment using the nondimensional distance y+ and the turbulent kinetic energy.

For a better understanding of the calculation results, preceding jets of unburned PC mixture and following torch flames should be distinguished from the ambient gas or the mixture in the MC. In the study, the gas components originating from the PC mixture were identified as marker gas.

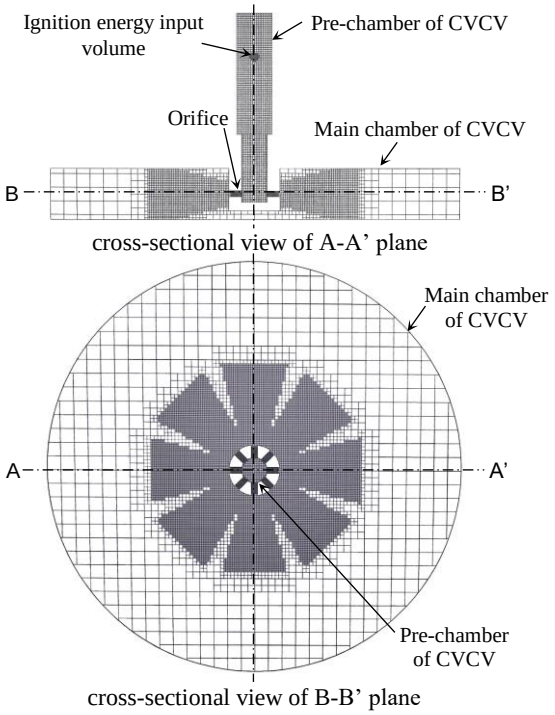

Fig. 2. Schematic view of initial meshing of the computational domain for the CVCV inner volume with a reference PC tip (Tip #1, see Table 3 and Fig. 3)

The jets of the unburned PC mixture were identified by setting the boundary concentration of marker gas to 1.0 mass%, and the torch flames including the ignited MC mixture were identified by setting the boundary cell temperature to 350 K or higher.

4. Experimental conditions

Table 2 lists the experimental conditions both for combustion tests and numerical simulations. Photographing setups for the combustion tests are also included in the lower lines of the table. Following the mixture formation in actual PC-type gas engines, the PC is always filled with a stoichiometric (λ_{PC} = 1.0) CH_4/air mixture to secure stable ignition and strong torch flame ejection. MC gas conditions, however, were determined by the experimental considerations. In the case of non-combustible MC gas, the MC is filled with pure nitrogen by shutting off both an oxygen valve for artificial air preparation in the primary supply line and a CH_4 valve in the secondary supply line. In the case of MC mixture gas, both the valves are open to prepare a CH_4/air mixture of an equivalence ratio of λ_{MC} = 1.7.

Table 2. Experimental conditions

Gas charging state	1.0 MPa, 300 K
Fuel gas in PC	CH_4/air premixture, λ_{PC} = 1.0
Ambient gas in MC	N_2 (non-combustible) CH_4/air premixture, λ_{MC} = 1.7
PC tips	#1~#8 on Table 3
Frame rate	20,000 fps
Resolution	1024×1024 pixels
Exposure time	10.0 μs

Figure 3 shows a cross-sectional view of the reference PC tip: Tip #1. As mentioned above, PC orifices are horizontally bored to make it easy to measure the penetration and spread cone angle of the torch flame from the visualized torch flame images through a quartz glass window covering the whole bottom surface of the MC.

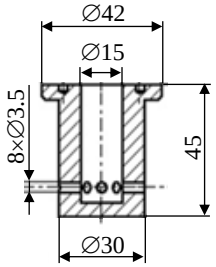

Fig. 3. Cross-sectional view of the reference PC tip (Tip #1, see Table 3)

Table 3 shows a specification list of eight PC tips identified as Tip ID: #1~#8. Tip #1 is selected as the reference PC tip, in which the orifice diameter; D_{ori} is ∅3.5 mm, and the number of orifices; N_{ori} is set to 8. Tips #2 and #3 have N_{ori} of 6 and 10, respectively, and their D_{ori} is determined so that the total orifice opening area is almost the same as that of Tip #1. For Tips #4 and #5, N_{ori} is set constant at 8 and D_{ori} is set to ∅2.5 mm and ∅5.0 mm, respectively.

Table 3. Main specifications of the PC tips

PC tip ID	Orifice specifications					Tip throat diameter D_{trt} [mm]	Chamber vol. ratio V_{PC}/V_{MC} [%]
	Diameter D_{ori} [mm]	Length L_{ori} [mm]	Aspect ratio $(L/D)_{ori}$ [-]	Number of holes N_{ori} [-]	Total opening area A_{ori} [cm^2]		
#1	∅3.5	7.5	2.14	8	0.770	∅15	2.3
#2	∅4.0	7.5	1.86	6	0.754	∅15	2.3
#3	∅3.1	7.5	2.42	10	0.755	∅15	2.3
#4	∅2.5	7.5	3.00	8	0.393	∅15	2.3
#5	∅5.0	7.5	1.50	8	1.571	∅15	2.3
#6	∅3.5	5.0	1.43	8	0.770	∅10	2.0
#7	∅3.5	7.5	2.14	8	0.770	∅10	2.0
#8	∅3.5	10.0	2.86	8	0.770	∅10	2.0

Each nozzle tip has a different orifice aspect ratio; $(L/D)_{ori}$ ranging from 1.43 to 3.00 and two variations of relative PC volume; V_{PC}/V_{MC} at 2.3% (Tips #1~#5) or 2.0% (Tips #6 ~#8).

5. Results and discussion

5.1. Analysis methodology

In a PC-type gas engine, combustion in an MC progresses due to the combination of the forced ignition by the torch flames and their mixing/combustion promotion effect on the MC mixture. To identify the above effects, the CVCV can switch the MC ambience to non-combustible pure nitrogen or methane-air premixture. Wakasugi et al. [22] carried out visualization measurements of the torch flame with the MC ambience under both non-combustible and combustible conditions.

In this study, however, as a first step in investigating the combustion process of PC-type gas engines, the reproducibility of numerical predictions regarding the influence of orifice specifications on torch flame ejection behaviour was evaluated by comparing measurement results in non-combustion conditions with numerical prediction results. Moreover, the preceding ejection process of unburned gas from the PC, which is difficult to observe with visualization experiments was numerically examined.

5.2. Effects of orifice aspect ratio

As explained, eight PC tips with different specifications were prepared to investigate the influence of orifice specifications, but changing only certain factors is not always easy and requires careful consideration of measurement results. First, the effects of the orifice aspect ratio; $(L/D)_{ori}$ were examined as an example of changing a single specific factor of a PC.

Figure 4 compares the temporal change of the penetration length and the spreading (cone) angle of the torch flame between the measurement results and the simulation results when only the aspect ratio was varied in a range of $(L/D)_{ori}$ = 1.43, 2.14, and 2.86 by changing L_{ori} = 5.0 mm (Tip #6), 7.5 mm (Tip #7), and 10.0 mm (Tip #8) respectively while keeping N_{ori} = 8, D_{ori} = ∅3.5 mm. Both values are averaged over the 8 torch flames from each orifice. The displayed time unit: ASOE represents the elapsed time since the torch flame started ejecting from the PC. Increasing the aspect ratio extends the penetration of torch flames and suppresses their spreading angle. Compared to diesel spray, a major feature of torch flame is that there is a high inverse correlation between ejection velocity and spread angle, but the tendency was relatively small in these cases because the ejected momentum was kept the same. It should be noted the discrepancy between measurements and numerical predictions is large in the early stage of the torch flame ejection, and the order of the penetration between $(L/D)_{ori}$ = 2.14 and 2.86 is reversed. It may be caused by the difficulty in determining the ignition of the unburned methane-air premixture preceding torch flames. In the visualization, the determination depends on how to distinguish the boundary between the unburned mixture and the torch flame based on the brightness of the shadowgraph image, and in the CFD calculation, it depends on the evaluation of the dilution effect by atmospheric nitrogen. Although the difference between the two decreases in the late stage of ejection as the momentum of the torch flame decreases, the influence of underestimation of the measurement seems more dominant (See arrows B and C in Fig. 5). As for the spreading angle of the torch flame, its trends versus $(L/D)_{ori}$ are said to be well reproduced both qualitatively and quantitatively.

Figure 5 compares the shadowgraph images of the torch flame and the visualized results of the numerical prediction. The black circle in the centre of the shadowgraph image corresponds to the bottom of the PC. The prediction results show the area where the temperature surpassed the threshold level in the horizontal cross-section B-B' in Fig. 2. Due to the insufficient adjustment of the optical system, false information was often superimposed in the shadowgraph images as a darkened area of about twice the PC radius around the PC (See arrow A in the figure). In addition, because of dividing the cylindrical combustion chamber of the CVCV with cubic cells, the predicted penetration and the shape of the torch flames tend to be different whether the direction of mesh division is perpendicular or oblique to the torch flame ejection.

5.3. Effects of throat diameter of nozzle tip

Second, the effects of the throat diameter of a nozzle tip; D_{trt} were checked as another example of changing a near single PC specification by replacing the reference PC Tip #1 (D_{trt} = ∅15 mm) with Tip #7 (∅10 mm). With this exchange, a PC/MC volume ratio; V_{PC}/V_{MC} was also reduced from 2.3 % to 2.0 % and the stored energy in the PC by 15%, and some throttling effect was given at the same time during the flame propagation from a main part of the PC to the PC tip.

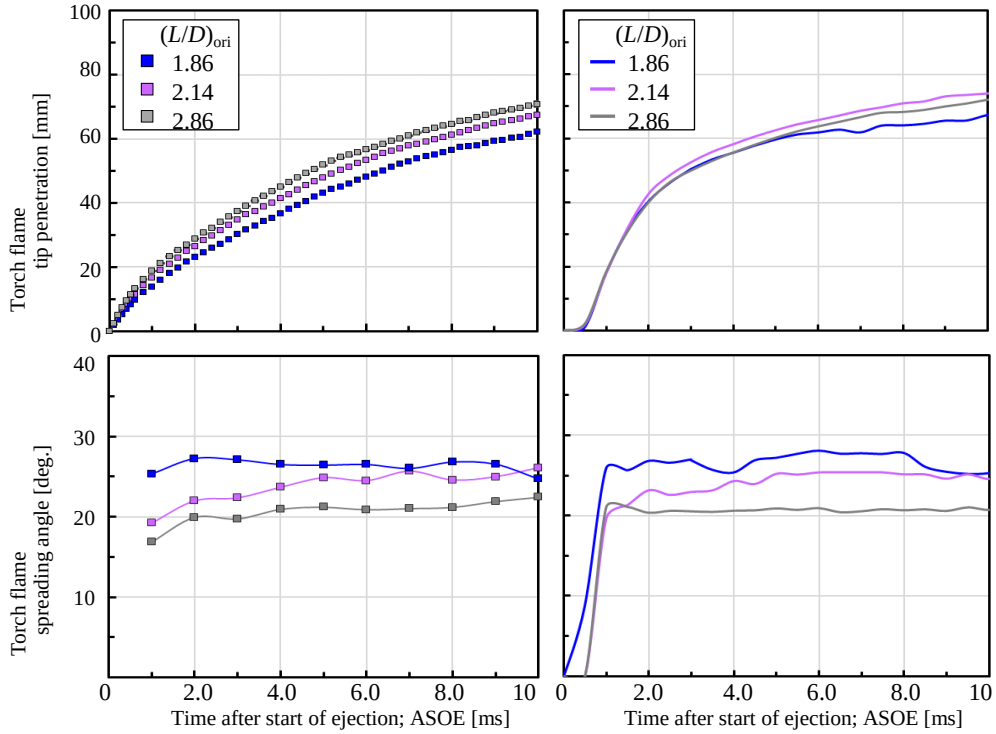

Fig. 4. Effects of $(L/D)_{ori}$ on torch flame penetration and its spreading angle by PC Tip #6 ($(L/D)_{ori}$ = 1.43), #7 (2.14), and #8 (2.86) respectively with N_{ori} = 8 and D_{ori} = ∅3.5 mm in common, measurement results (left half), and simulation results (right half)

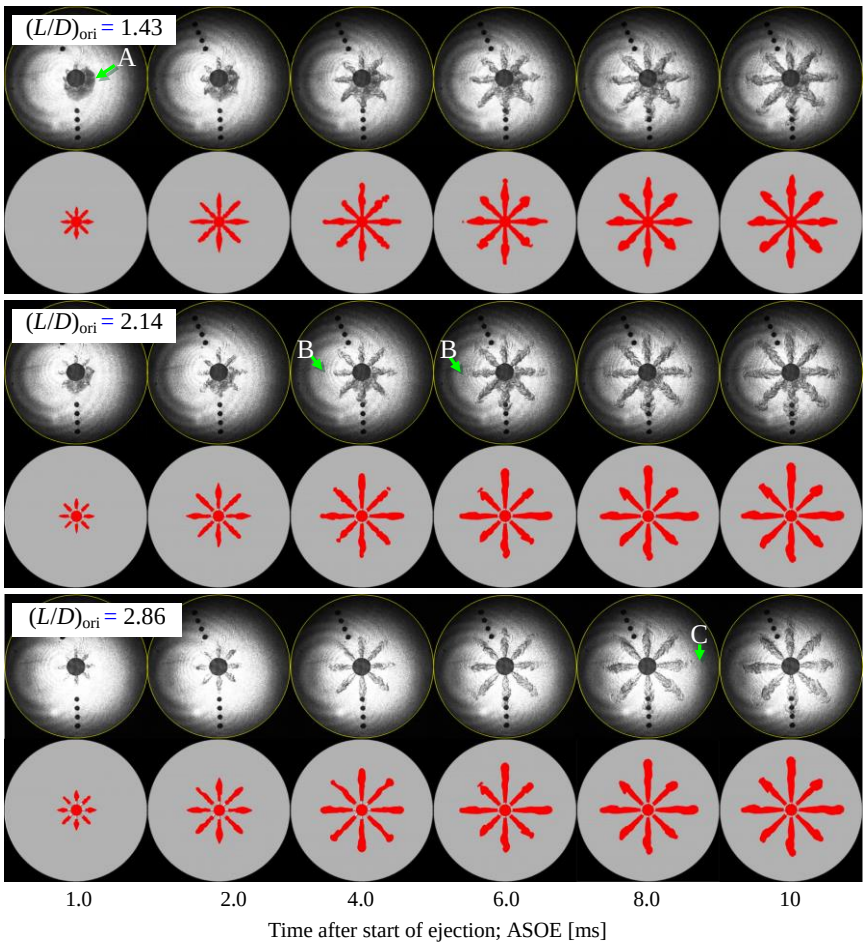

Fig. 5. Effects of orifice aspect ratio; $(L/D)_{ori}$ on ejection behaviour of torch flame by PC Tip #6 ($(L/D)_{ori}$ = 1.43), #7 (2.14), and #8 (2.86) respectively with N_{ori} = 8 and D_{ori} = ∅3.5 mm in common, shadowgraph images (upper row of island), and simulation results (lower row)

Figure 6 shows the temporal change of the penetration length and the spreading angle of the torch flame comparing the measurement and simulation results. All in all, the decrease in D_{trt} was observed to cause a slower ejection speed from the PC orifice and a wider spreading angle of the torch flame. The agreement of both results was qualitatively good in these aspects, but the torch flame penetration was overestimated especially in the jet-developing process of the D_{trt} = ∅10 mm (V_{PC}/V_{MC} = 2.0%) case. The numerical simulation in the study may overestimate the heat release rate in the PC and the exaggeration of the throttling effect. These suggest that not only the stored energy in the PC but also the combustion process and the cross-sectional shape are important for predicting the ejection behaviour of torch flame.

5.4. Effects of number of orifices

Third, the effects of N_{ori} on torch flame behaviour were preferentially explored because the number of orifices is an important design factor in a PC-type gas engine. It directly affects the torch flame distribution and the ignition area in the MC mixture. In the study, N_{ori} was set to 6 (Tip #2), 8 (Tip #1), and 10 (Tip #3) with the total orifice opening area; A_{ori} and the PC volume; V_{PC} kept almost constant. So, D_{ori} changed to ∅4.0 mm, ∅3.5 mm, and ∅3.1 mm, and $(L/D)_{ori}$ changed to 1.86, 2.18, and 2.42 for the N_{ori} = 6, 8, and 10 orifice cases, respectively.

Figure 7 and 8 summarize the measurement and simulation results in the same manner as the previous case. The false information was superimposed again in the shadowgraph images of the N_{ori} = 10 case (See arrow A). Since the momentum of a single torch flame is inversely proportional to N_{ori}, the N_{ori} = 6 case shows the longest penetration and the N_{ori} = 10 shows the shortest. However, the torch flame penetration showed little difference until about 1 ms ASOE in all cases, then the growth gradient for the 10-orifice case got slower around the timing, and the 6-orifice case showed a similar behaviour at about 6 ms ASOE. This trend can be attributed to the momentum of the individual torch flames. The torch flame led by unburned gas in the PC has a sharper tip than two-phase diesel sprays. It suggests the preceding unburned PC mixture could assist the torch flame penetration before slowing down claimed by Zhou et al. [25].

The overall reproducibility of the torch flame behaviour by the CFD of the study shows good agreement with these characteristics of the torch flame. Moreover, prediction results for 2 ms ASOE with N_{ori} = 6 hinted that the torch flames located in up and down directions in Fig. 6 partially quenched at their tip and an unburnt region remains in the centre of the tip even after flame development, indicating that the ejection intensity of the torch flame can affect the combustion process in the MC (See arrow B). Although the prediction results successfully reproduce effects on the penetration and spreading angle of the torch flame, as well as their order among the tested N_{ori}s, the predictions overestimate the penetration up to around 2 ms ASOE in the early

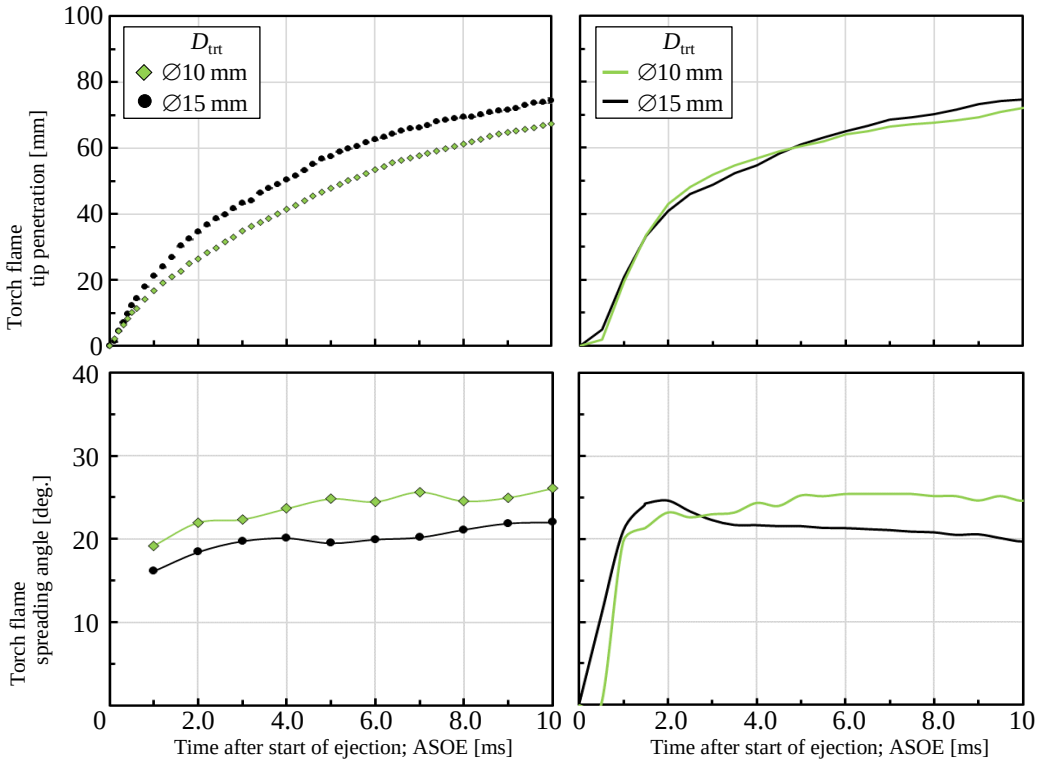

Fig. 6. Effects of D_{trt} n torch flame penetration and its spreading angle by PC Tip #1 (D_{trt} = ∅15 mm, V_{PC}/V_{MC} = 2.3%) and #7 (∅10 mm, 2.0%) respectively with N_{ori}(= 8) and L_{ori}(= 7.5 mm) in common, measurement results (left half), and simulation results (right half)

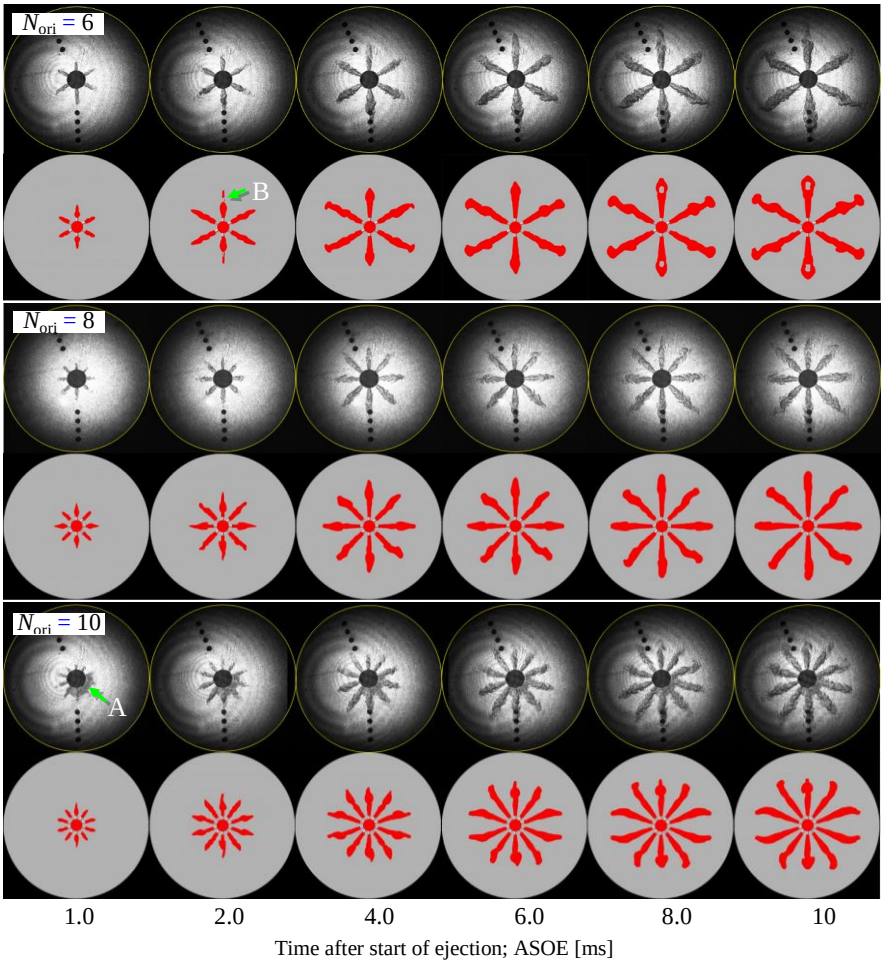

Fig. 7. Effects of number of orifices; N_{ori} on ejection behaviour of torch flame by PC Tip #2 (N_{ori} = 6, D_{ori} = ∅4.0 mm), #1 (8, ∅3.5 mm), and #3 (10, ∅3.1 mm) respectively, with ca. same A_{ori}, measurement results (upper row of island), and simulation results (lower row)

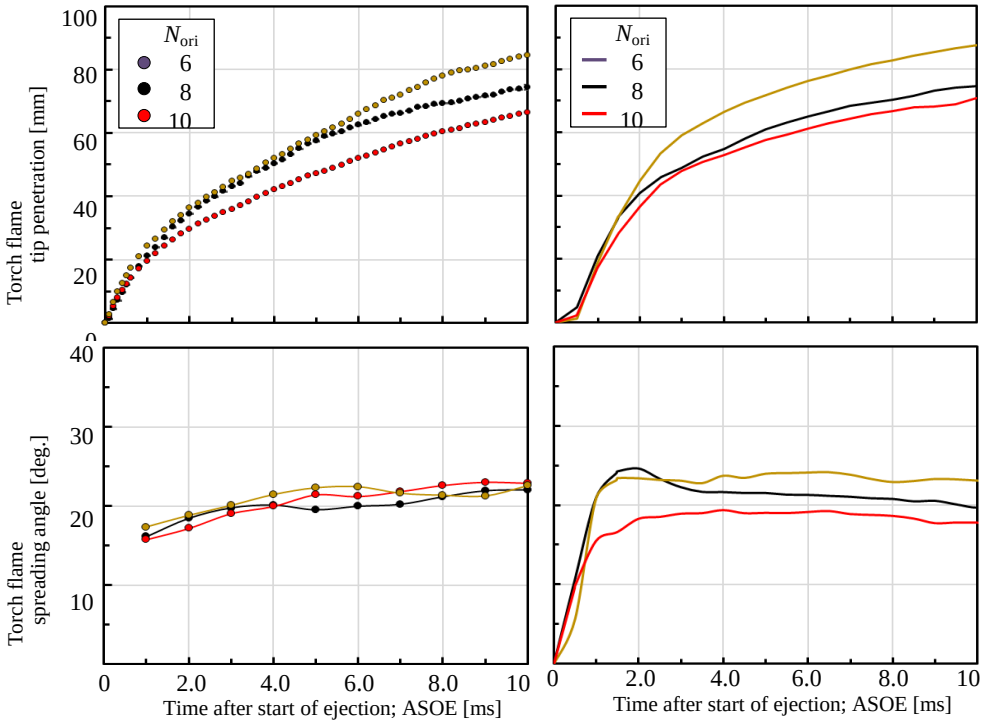

Fig. 8. Effects of N_{ori} on torch flame penetration and its spreading angle by PC Tip #2 (N_{ori} = 6, D_{ori} = ∅4.0 mm), #1 (8, ∅3.5 mm), and #3 (10, ∅3.1 mm) respectively, with ca. same A_{ori}, measurement results (left half), and simulation results (right half)

images that as D_{ori} increases, the penetration of the torch flame decreases and the spreading angle after the torch development increases. Unlike the previous experiments with almost constant A_{ori}, there was a clear difference among the penetrations of the three cases immediately after the ejection. This can be explained by the fact that the ejection speed of the torch flame from orifices could be roughly in inverse proportion to A_{ori} or square of D_{ori}, since the combustion process in the PC is thought to be the same regardless of the nozzle tip specifications.

5.5. Effects of orifice diameter

Finally, the effects of the orifice diameter: D_{ori} were investigated by changing the reference Tip #1 to Tip #4 or Tip #5. D_{ori} was ∅2.5 mm in Tip #4, ∅3.5 mm in Tip #1, and ∅5.0 mm in Tip #5 keeping N_{ori}(= 8), L_{ori}(= 7.5 mm), and V_{PC}/V_{MC}(= 2.3%) at their reference values. The ratio of A_{ori} among these PC tips was about 1: 2: 4, and $(L/D)_{ori}$ changed from 3.00 through 2.14 to 1.50. So, the effects of $(L/D)_{ori}$ should be counted when considering both experimental results.

Figure 9 and 10 summarize the measurement and simulation results. Again, arrow A in a shadowgraph image of the D_{ori} = ∅5.0 mm case shows that the false information was include. It can be seen in the shadowgraph stage of ejection and the effects of N_{ori} on the spreading angle. The latter may reflect the larger flame contour variation with jetting momentum in the spread angle.

Both the measurement and simulation results showed good qualitative agreement with the above behaviour, but they do not match quantitatively very well except for the reference case of Tip #1. The penetration length was unignorably underpredicted in the D_{ori} = ∅2.5 mm case and overestimated in the D_{ori} = ∅5.0 mm case while the spreading angle was underestimated in the latter case. The reason may be that the prediction in this study does not accurately reflect the stretching and misfiring of a reaction zone varied on the ejection speed of the torch flame. In other words, in the D_{ori} = ∅2.5 mm case, the ignitability of the preceding PC mixture may be underestimated compared to the measurement results. In contrast, it may be overestimated in the D_{ori} = ∅5.0 mm case. All of these imply the importance of investigating the behaviour of unburned gas that precedes the torch flame. This will be discussed in detail later.

5.6. Effects of unburned PC mixture ejection

Figure 11 is an example of the PC configuration of 4-stroke-cycle lean-burn gas engines. Since the 4-valve layout is necessary for high-power-density engines, the PC should be in the centre of the combustion chamber, have a funnel shape expanding upward, and locate the fuel supply port and the spark plug on its top surface. This means the ignited flame in the PC always propagates from top to bottom and a considerable portion of the methane-air mixture inside the PC is discharged being unburned before the torch flame ejection. This preceding PC mixture can be the origin of the difference between the measured torch flame penetration and the predicted one.

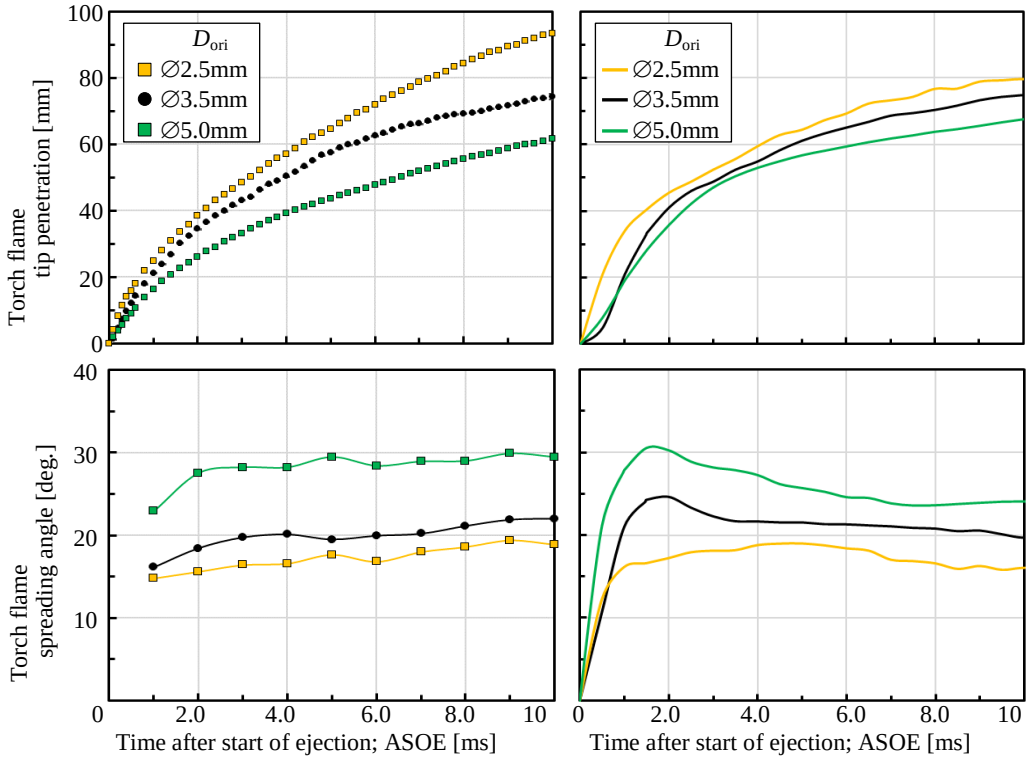

Fig. 9. Effects of D_{ori} = ∅2.5 mm, ∅3.5 mm, and ∅5.0 mm on torch flame penetration and its spreading angle by PC Tip #4, #1, and #5 respectively with N_{ori}(= 8) and V_{PC} in common, measurement results (left half), and simulation results (right half)

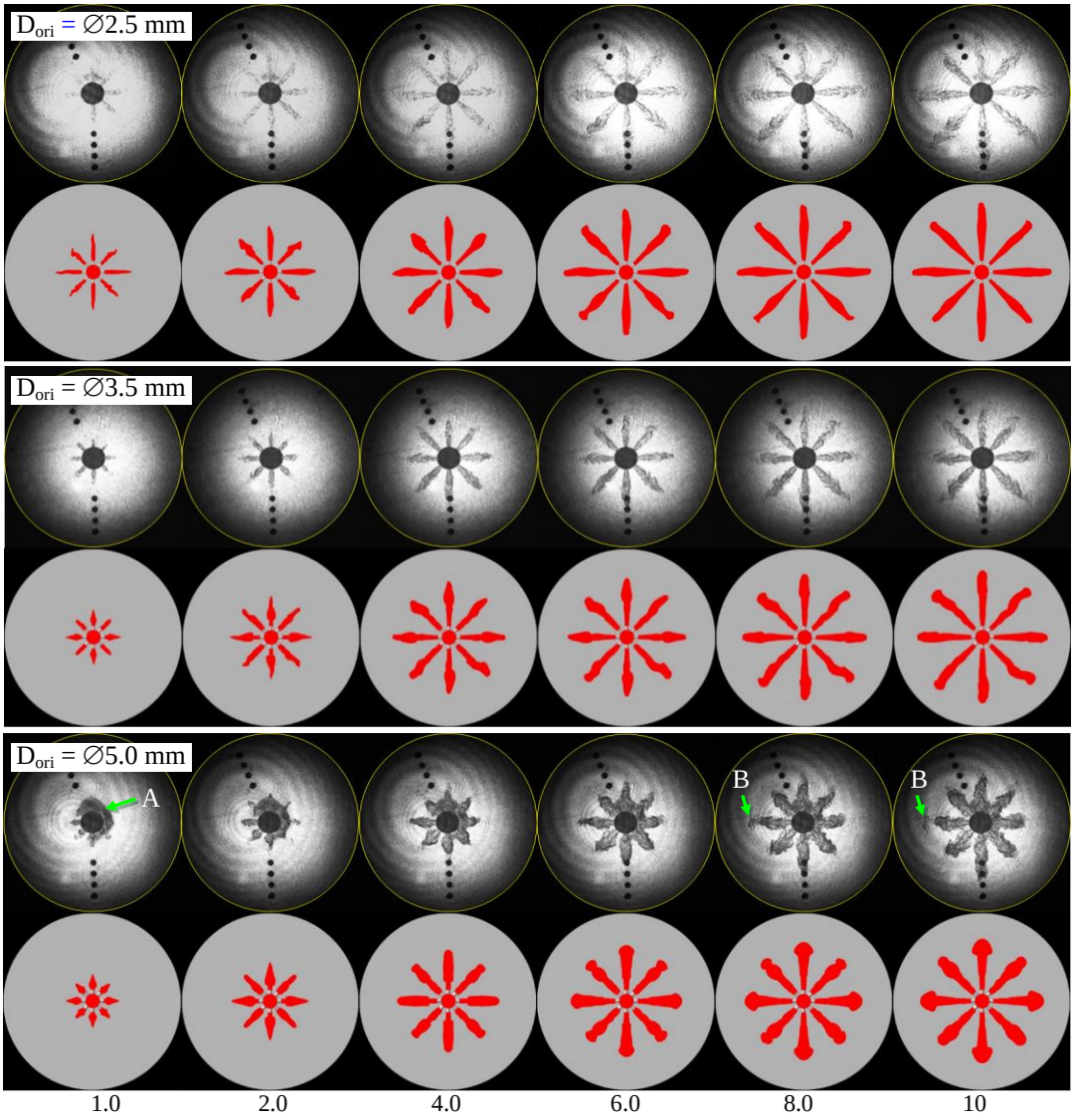

Fig. 10. Effects of orifice diameter; D_{ori} on ejection behaviour of torch flame by PC Tip #4 (∅2.5 mm), #1 (∅3.5 mm), and #5 (∅5.0 mm), respectively with N_{ori} = 8 and V_{PC} in common, in the shadowgraph images (upper row of island) and simulation results (lower row)

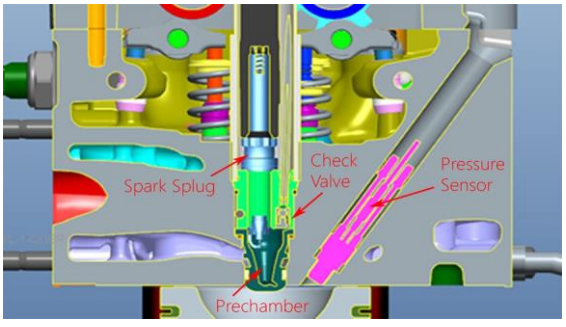

Fig. 11. Example of cross-sectional view of pre-chamber assembly [4]

Figure 12 compares enlarged views of observed plumes of unburned PC mixture in the N_{ori} = 10 case with corresponding ones predicted by the CFD. The latter was visualized as the light yellow iso-surface of 1 mass% of the PC mixture (marker gas). The arrows in the shadowgraph images indicate the position of the visible jet tips of the unburned PC mixture. The capture timings of the two are not the same due to the difference in storage period. The CFD gave so quick diffusion of the PC mixture into the MC in advance that the mixture surrounded the outer circumference of the PC before the ejection was captured in the shadowgraph at 16.0 ms ASOE. After the true ejection started, however, penetrations of both experiments seemed the same, and their variation among the orifices seemed small. Since the diffusion to the MC ambient means dilution of the preceding PC mixture with inert nitrogen, it is expected to affect the ignitability of the mixture by the following torch flame.

Figure 13 collects the predicted behaviours of torch flame from the investigation for the effect of D_{ori} with light yellow iso-surfaces of the PC mixture superimposed. As mentioned in Fig. 11, there was a discrepancy in penetration length between the observed and predicted torch flame, which is presumably due to the lack of reproducibility in the entrainment of MC ambient by the ejected PC mixture

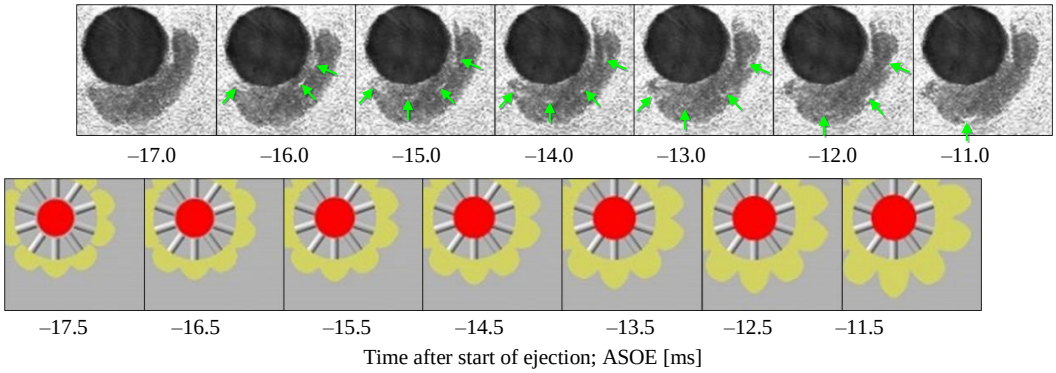

Fig. 12. Enlarged view of the ejection process of the unburned PC premixture by PC Tip #3 (N_{ori} = 10, D_{ori} = ∅3.1 mm), measurement results (upper row), and simulation results (lower row), arrows in the shadowgraph images

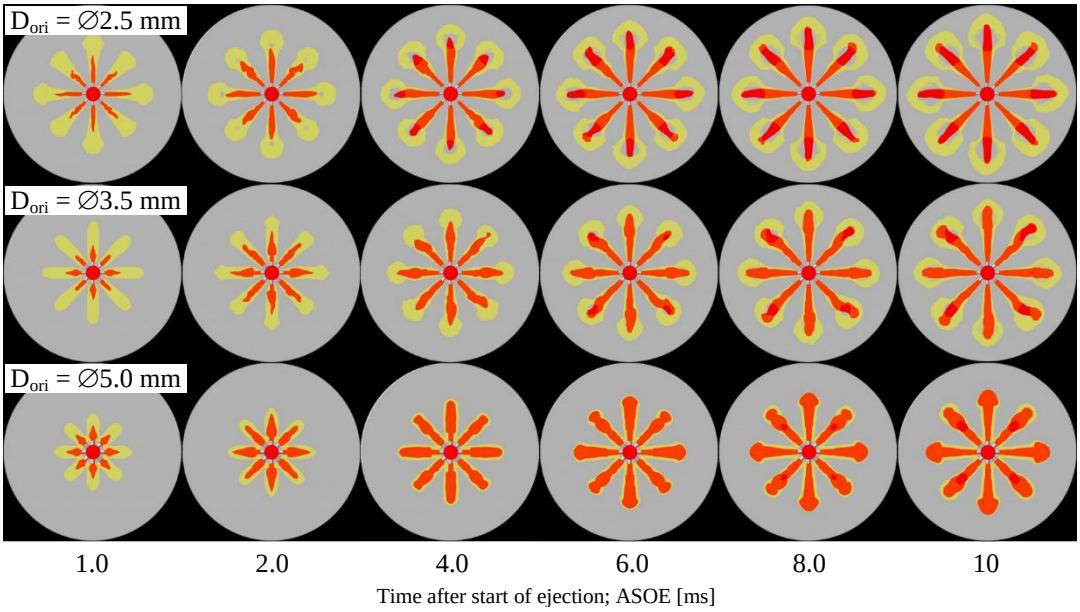

Fig. 13. Predicted relation between the preceding plumes of unburned premixture and the following torch flames by PC Tip #4 (D_{ori} = ∅2.5 mm), #1 (∅3.5 mm), and #5 (∅5.0 mm), respectively with N_{ori} = 8 and V_{PC} in common

and in the ignition occurrence from the torch flame. In general, the higher ejection speed enhances the MC nitrogen entrainment of the PC mixture and the stretch of the torch flame, and results in the deterioration of the ignitability of the torch flame to the plume of the PC mixture. In the D_{ori} = ∅2.5 mm case, the preceding PC mixture has the highest ejection velocity of the three cases, and its entrainment of MC nitrogen progresses since the tip of the premixture decelerates and expands because of the entrainment by the time the torch flame starts ejection. The torch flame also decelerates significantly as the torch flame travels through the unburned premixture, but no ignition of the premixture occurs from the torch flame.

On the other hand, in the D_{ori} = ∅5.0 mm case, the unburned premixture is ignited as early as 2 ms after the torch flame ejection, and the flame length increases rapidly, after which the torch flame progresses almost entirely into the premixture. By Comparing with the combustion visualization by the shadowgraph, it is thought that the ignitability of the premixture by the torch flame was underestimated in the former case and overestimated in the latter.

6. Conclusions

In this study, the effects of specifications of a pre-chamber (PC) tip were numerically examined in detail based on the comparison with measurement results in a constant-volume combustion vessel (CVCV) that simulated the combustion chamber configuration of a medium-speed PC-type gas engine. As a first step in investigating the combustion process of PC-type gas engines, the reproducibility of CFD predictions regarding the influence of PC tip specifications on torch flame ejection was evaluated under non-combustion conditions by charging pure nitrogen in the main chamber (MC). Moreover, the preceding ejection process of unburned premixture from the PC was discussed in some cases succeeding in its visualization. The following conclusions were obtained.

1. The reproducibility of the CFD simulation that considers the reduction of calculation load for the application to a medium-speed gas engine was successfully evaluated based on measurement results of the torch flame behaviour in a constant-volume combustion vessel (CVCV) with the same scale as a PC-type medium-

speed gas engine under non-combustible ambient conditions in an MC.

2. If other specifications of the PC tips are the same, the penetration length of torch flames of a PC-type gas engine is proportional to the ejection velocity or the ejection momentum of a torch flame, while their spreading angle changes inversely. The trends were qualitatively and quantitatively reproduced by the applied CFD frame. Although the increase in the orifice aspect ratio and the decrease in the PC tip throat diameter also give similar but relatively weaker trends, the reproducibility of the numerical simulation got worse with these parameters.
3. The numerical predictions consistently tended to overestimate the penetration of the torch flame in the early stage of the ejection. The discrepancy is probably attributed to the unburned premixture ejection from the PC preceding the torch flame. For the applied shadowgraph optics in the measurements, it was difficult to identify the ignited region of the unburned premixture by the torch flame, and for the applied numerical prediction, it was difficult to reproduce the entrainment of the MC ambient and the ignition process of the unburned premixture.
4. The investigation of the effects of a PC orifice diameter showed that the ignition potential of the torch flame tended to be overestimated in the larger orifice case of a slower ejection speed and less MC ambient entrainment, but it was reversed in the smaller orifice case of a higher ejection speed. As for the tip penetration of the unburned premixture, detailed observation of the shadowgraph images and the visualized prediction results were in good agreement, but the simulated penetration was somewhat obscure because of the excessive numerical diffusion of the premixture from the orifice into the MC ambient and the evaluation uncertainty in the ignitability of the nitrogen-diluted unburned premixture by the torch flame.

As a next step, it is necessary to simulate the whole combustion process numerically with the MC charged with a lean premixture of CH_4/air. By comparing with the experimental results in the MC combustion cases by Wakasugi et al. [22], essential flame propagation from the torch flame surface into the MC premixture would be numerically clarified, and then a novel and practical index for the combustion-promoting potential of the torch flame such as so-called “jet intensity” could be formulated based on the PC tip specifications.

Nomenclature

A_{ori}	total opening area of PC tip orifices
AMR	adaptive mesh refinement
ASOE	after the start of ejection
CFD	computational fluid dynamics
CN	carbon neutrality
CPU	central processing unit
CVCV	constant volume combustion vessel
D_{ori}	diameter of PC orifice
D_{trt}	throat diameter of PC tip
GHG	greenhouse gas
GRI	Gas Research Institute
IMO	International Maritime Organization
L_{ori}	length of PC orifice
$(L/D)_{ori}$	aspect ratio of PC tip orifice
MC	main combustion chamber
MEPC	Marine Environment Protection Committee
N_{ori}	the number of PC tip orifices
NG	natural gas
NO_x	nitrogen oxides
PC	pre-combustion chamber
RANS	Reynolds-Averaged Navier-Stokes equations
SAGE	structural adaptive grid embedding
SI	spark ignition (forced ignition)
t	tickness of oprical window
TJI	turbulent jet ignition
V_{MC}	capacity volume of MC
V_{PC}	capacity volume of PC
λ_{PC}	global air excess ratio in PC
λ_{MC}	global air excess ratio in MC

Bibliography

[1] Aakko-Saksa T, Lehtoranta K, Kuittinen N, Järvinen A, Jalkanen J, Johnson K et al. Reduction in greenhouse gas and other emissions from ship engines: current trends and future options. Prog Energ Combust. 2023;94:101055. https://doi.org/10.1016/j.pecs.2022.101055

[2] Abdelhameed E, Tsuru D, Tashima H, Sako T, Consideration of combustion improvements of lean-burn gas engine with pre-combustion chamber. 30th CIMAC World Congress, Busan 2023.

[3] Atis C, Chowdhury SS, Ayele Y, Stuecken T, Schock H, Voice AK. Ultra-lean and high EGR operation of dual mode, turbulent jet ignition (DM-TJI) engine with active pre-chamber scavenging. SAE Technical Paper 2020-01-1117. 2020. https://doi.org/10.4271/2020-01-1117

[4] Bach C. Record efficiency for a gas engine. Empa HP. https://www.empa.ch/web/s604/gason

[5] Badr O, Alsayed N, Manaf M. A parametric study on the lean misfiring and knocking limits of gas-fueled spark ignition engines. Appl Therm Eng. 1998;18(7):579-594. https://doi.org/10.1016/S1359-4311(97)00029-X

[6] Falkner R. The Paris Agreement and the new logic of international climate politics. Int Aff. 2016;2(5):1107-1125. https://doi.org/10.1111/1468-2346.127086

[7] Guo H, Zhou S, Shreka M, Feng Y. Effect of pre-combustion chamber nozzle parameters on the performance of a marine 2-stroke dual fuel engine. Processes. 2019;7(12):876. https://doi.org/10.3390/pr7120876

[8] Keenan M, Pickett R, Tronconi E, Nova I, Kinnunen N, Suvanto M et al. The catalytic challenges of implementing a Euro VI heavy duty emissions control system for a dedicated lean operating natural gas engine. Top Catal. 2019;62:273-281. https://doi.org/10.1007/s11244-018-1127-7

[9] Kim J, Scarcelli R, Som S, Shah A, Biruduganti MS, Longman DE. Numerical investigation of a fueled pre-chamber spark-ignition natural gas engine. Int J Engine Res. 2022; 23(9):1475-1494. https://doi:10.1177/14680874211020180
[10] Korakianitis T, Namasivayam AM, Crookes RJ. Natural-gas fueled spark-ignition (SI) and compression-ignition (CI) engine performance and emissions. Prog Energ Combust. 2011;37(1):89-112. https://doi.org/10.1016/j.pecs.2010.04.002
[11] Kulzer AC. Sustainability & powertrain systems: from electrification to hydrogen and eFuels (updated). Proc. JSAE PEL Int Meeting, Technical Challenges for a Carbon Neutral Society by 2050. Kyoto 2023.
[12] IMO HP MEPC80. https://www.imo.org/en/MediaCentre/PressBriefings/pages/Revised-GHG-reduction-strategy-for-global-shipping-adopted-.aspx
[13] Liyan F, Jun Z, Bo L, Lei C, Weiyao W, Long W et al. Research on the characteristics of enrichment fuel injection process in the pre-chamber of a marine gas engine. SAE Technical Paper 2015-01-1961. 2015. https://doi.org/10.4271/2015-01-1961
[14] Matla J, Kaźmierczak A, Haller P, Trocki M. Hydrogen as a fuel for spark ignition combustion engines – state of knowledge and concept. Combustion Engines. 2024;196(1): 73-79. https://doi.org/10.19206/CE-171541
[15] Sadanandan R, Markus D, Schießl R, Maas U, Olofsson J, Seyfried H et al. Detailed investigation of ignition by hot gas jets. P Combust Inst. 2007;31(1):719-726. https://doi.org/10.1016/j.proci.2006.08.027
[16] Senecal PK, Pomraning E, Richards KJ. Multi-dimensional modeling of direct injection diesel spray liquid length and flame lift-off length using CFD and parallel detailed chemistry. SAE Technical Paper 2003-01-1043. 2003. https://doi.org/10.4271/2003-01-1043
[17] Shapiro E, Tiney N, Kyrtatos P, Kotzagianni M, Bolla M, Boulouchos K et al. Experimental and numerical analysis of pre-chamber combustion systems for lean burn gas engines. SAE Technical Paper 2019-01-0260. 2019. https://doi.org/10.4271/2019-01-0260
[18] Tashima H, Kunimitsu M, Sugiura K, Tsuru D. Development of high-efficiency gas engine through observation and simulation of knocking phenomena. 26th CIMAC World Congress, Bergen 2010.
[19] Trombley G, Toulson E. A fuel-focused review of pre-chamber initiated combustion. Energ Convers Manage. 2023; 298:117765. https://doi.org/10.1016/j.enconman.2023.117765
[20] Validi AA, Schock H, Jaberi F. Turbulent jet ignition assisted combustion in a rapid compression machine. Combust Flame. 2017;186:65-82. https://doi.org/10.1016/j.combustflame.2017.07.032
[21] Valladolid PG, Tunestål P, Monsalve-Serrano J, García A, Hyvönen J. Impact of diesel pilot distribution on the ignition process of a dual fuel medium speed marine engine. Energ Convers Manage. 2017;149:192-205. https://doi.org/10.1016/j.enconman.2017.07.023
[22] Wakasugi T, Tsuru D, Tashima H. Influences of the pre-chamber orifices on the combustion behavior in a constant volume chamber simulating pre-chamber type medium-speed gas engines. Combustion Engines. 2022;191(4):66-76. https://doi.org/10.19206/CE-148171
[23] Yasueda S, Takasaki K, Tashima H. The abnormal combustion affected by lubricating oil ignition in premixed gas engine, Proceedings of the ASME 2012 Internal Combustion Engine Division Spring Technical Conference. 2012:29-36. https://doi.org/10.1115/ICES2012-81042
[24] Ye Y, Yue Z, Wang H, Liu H, Wu C, Yao M. A mapping approach for efficient CFD simulation of low-speed large-bore marine engine with pre-chamber and dual-fuel operation. Energies. 2021;14(19):6126. https://doi.org/10.3390/en14196126
[25] Zhou L, Song Y, Hua J, Liu F, Liu Z, Wei H. Effects of different hole structures of pre-chamber with turbulent jet ignition on the flame propagation and lean combustion performance of a single-cylinder engine. Fuel. 2022;308: 121902. https://doi.org/10.1016/j.fuel.2021.121902

Takahide Aoyagi, MEng. – Energy Conversion Group, Technology Platform Center, Technology & Intelligence Integration, IHI Corporation, Japan.
e-mail: *t.jr.aoyagi@gmail.com*

Daisuke Tsuru, DEng., Ass. Prof. – Shipping Technology Department, National Institute of Technology Oshima College, Japan.
e-mail: *tsuru.daisuke@oshima.kosen-ac.jp*

Takuya Wakasugi, MEng. – Interdisciplinary Graduate School of Engineering Sciences, Kyushu University, Japan.
e-mail: *wakasugi.takuya.875@s.kyushu-u.ac.jp*

Hiroshi Tashima, DEng., Ass. Prof. – Faculty of Engineering Sciences, Kyushu University, Japan.
e-mail: *tajima.hiroshi.539@m.kyushu-u.ac.jp*